

# Isolated Post Resonator Mesogyroscope

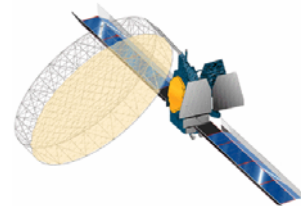
Dorian Challoner<sup>1</sup>, Saverio D’Agostino<sup>2</sup>, Chris Peay<sup>2</sup>, Joanne Wellman<sup>2</sup>, Kirill Shcheglov<sup>2</sup>, Ken Hayworth<sup>2</sup>, Dean Wiberg<sup>2</sup>, Karl Yee<sup>2</sup>

<sup>1</sup>Boeing Satellite Systems  
W/EO1/D111  
2000 E. El Segundo Blvd, El Segundo, CA 90245  
310-416-5219  
[anthony.d.challoner@boeing.com](mailto:anthony.d.challoner@boeing.com)

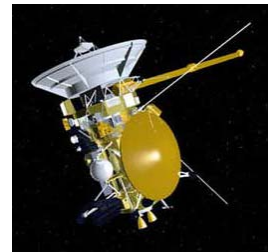
<sup>2</sup>Jet Propulsion Laboratory  
4800 Oak Grove Dr., Pasadena, CA91109

*Abstract*— A new symmetric vibratory gyroscope principle has been devised in which a central post proof mass is counter-rocked against an outer sensing plate such that the motion is isolated from the gyroscope case. Prototype gyroscopes have been designed and fabricated with micromachined silicon at mesoscale (20-cm resonator width), vs. microscale (e.g., 2-mm resonator width) to achieve higher sensitivity and machined precision. This novel mesogyro design arose out of an ongoing technical cooperation between JPL and Boeing begun in 1997 to advance the design of micro-inertial sensors for low-cost space applications. This paper describes the theory of operation of the mesogyro and relationships with other vibratory gyroscopes, the mechanical design, closed loop electronics design, bulk silicon fabrication and packaged gyroscope assembly and test methods. The initial packaged prototype test results are reported for what is believed to be the first silicon mesogyroscope. This development is being supported by the Defense Advanced Research Projects Agency.

## 1. INTRODUCTION



Thuraya



Cassini

### TABLE OF CONTENTS

.....	
<b>1. INTRODUCTION</b> .....	1
<b>2. MECHANICAL DESIGN</b> .....	3
<b>3. ELECTRICAL DESIGN</b> .....	4
<b>4. SILICON FABRICATION</b> .....	6
<b>5. ASSEMBLY &amp; PACKAGING</b> .....	7
<b>6. TEST METHODS &amp; RESULTS</b> .....	8
<b>7. CONCLUSIONS</b> .....	9
<b>REFERENCES</b> .....	9

Figure 1-1: Artificially-stabilized Aerospace Vehicles

Man’s conquest of air and space over the last century has driven the need for artificial stabilization of vehicle orientation. Today’s large vehicles pictured in Figure 1-1 now appear to be effortlessly oriented but man’s final defeat of gravity has been a supreme feat requiring very sophisticated attitude stabilization and control as well as lift. For such free-flying vehicles that can no longer enjoy the exquisite passive stability of our large planet Earth, artificial stabilization based on inertial sensors, e.g. gyroscopes, is quite appealing. Other possibilities, e.g. passive spin stabilization or optical reference sensors, pose significant mechanical limitations, complexity, external dependencies or computational challenges. Yet despite the inherent robustness of inertial stabilization and the availability of

high quality gyroscopes very few vehicles, especially small aerospace vehicles, have employed this method because of prohibitive size and cost of today's inertial sensors with adequate performance.

With the emergence of small micromachined vibratory gyroscopes that can potentially be mass produced with requisite precision, a revolution in air and space travel, especially for small vehicles is thus anticipated. Numerous mm-scale capacitive silicon micromachined gyroscopes have been advanced over the past ten to fifteen years [1]. Small discrete piezo-quartz tuning fork gyros have been manufactured [2] and tunneling-based vibratory gyroscopes have been advanced [3]. However, much of this effort is targeting very high volume commercial terrestrial applications such as automobile stabilization and appears to fall several orders of magnitude short of the performance needed for aerospace stabilization and navigation.



Figure 1-2: Hemispherical Resonator Gyroscope

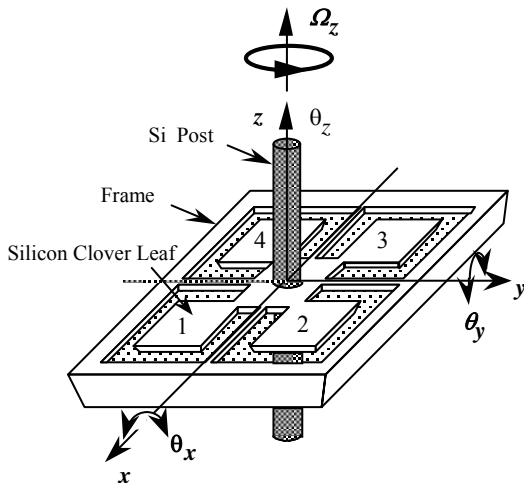


Figure 1-3: Cloverleaf-Post microgyroscope

One vibratory gyroscope design with navigation grade performance, the quartz hemispherical resonator gyro (HRG) was successfully selected in 1994 by Boeing for the

Telemetry Data Relay Satellite (TDRS). However, its 3D 30 mm fused quartz resonator, Figure 1-2, was conventionally machined to high precision so was unusually expensive to make. For future mission cost saving to enable new micro-satellites Boeing and JPL began to cooperate in 1997 on the performance advancement of the silicon cloverleaf microgyro, Figure 1-3. A unique characteristic of this design was the four thin cloverleaves attached to the central rocking post providing a large area sense capacitance. One degree per hour closed loop performance was demonstrated in early 1999 with our 4 mm wide silicon cloverleaf resonator. This was still noticeably short of the 0.01 deg/h achieved by the HRG.

A hypothesis for the performance shortfall was the potential loss in micro-machining precision resulting from the thin (26 micron) epitaxial silicon beams used in the cloverleaf microgyro. When DARPA Defense Sciences Office raised the question in 1999 of whether mesoscale (cm to fist size) would be more advantageous for certain militarily important devices we proposed to investigate a cm-scale silicon micromachined vibratory gyroscope based on our mm-scale cloverleaf microgyro[4]. Analysis of some preliminary designs showed that 3D micro-machined precision and resulting gyro performance would be improved by perhaps two orders of magnitude. A successful initial silicon fabrication feasibility study at mesoscale was followed by a mesogyroscope proof of concept demonstration in a vacuum chamber for DARPA/DSO and a packaged mesogyro demonstration for DARPA/SPO with a goal this year of 0.1 deg/h in-run ambient bias stability.

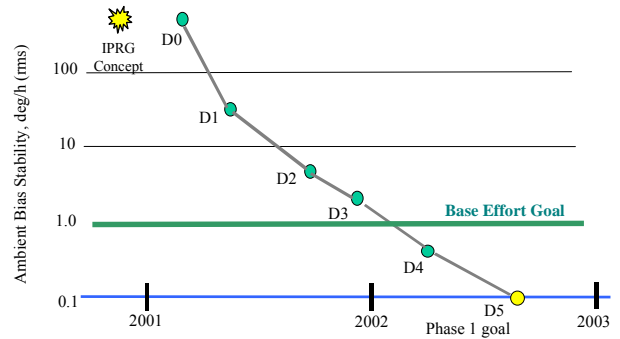
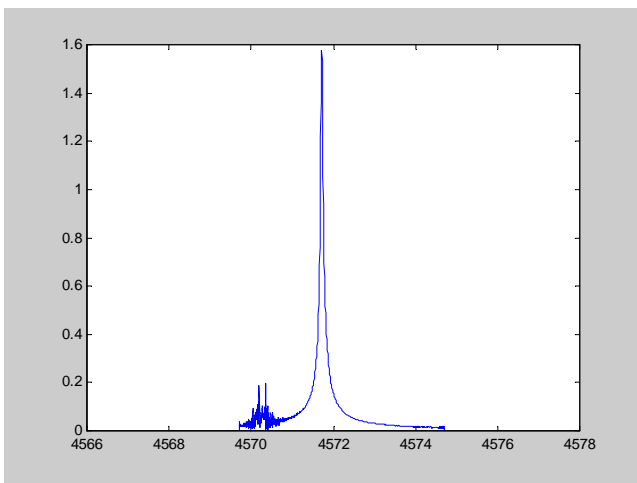


Figure 1-4: Mesogyro development timeline

The rapid progress of our development, charted in Figure 1-4 started with the Isolated Plate-Post Resonator Gyro concept resulted in a final packaged design that met our performance goal in less than two years. This paper describes the first mesoscale micromachined gyroscope, its development background, unique theory of operation, mechanical and electrical design, silicon fabrication method, assembly and packaging approach and a presentation of our test methods and results.

## 2. MECHANICAL DESIGN

A principal development objective was to significantly improve micromachining relative precision and thereby mesogyro performance. Our 4 mm scale micromachined cloverleaf with 25 micron thick beams exhibited a typical asymmetry or frequency split of 10 Hz between the two 3 kHz rocking modes or 0.33%. A double-side polished, through-etched 500 micron thick resonator with the basic cloverleaf resonator geometry (without post) was fabricated at 20 mm scale and suspended in vacuum with very fine strings. Electrostatic excitation and optical readout tests verified a frequency split as low as 0.1 Hz or <0.0033% matching at basic resonator level, as shown in Figure 2-1. This mesoscale resonator was thus 100X better matched than our microgyro resonator.



$$f_0 = 4571.7 \text{ Hz}, \Delta f < 0.1 \text{ Hz}, Q > 83,000$$

Figure 2-1: Mesoscale resonator precision

Scaling of the 500 micron wafer thick seismic frame of the 4 mm cloverleaf microgyro was not desirable at mesoscale for economic reasons. However, proportionately thinner frames were found at mesoscale to have undesirable high losses to the package. This then resulted in the conception of a novel mesogyroscope principle referred to as the isolated plate-post resonator gyro (IPPRG) or more simply the isolated post resonator gyro (IPRG).

Its overall construction and principle of operation is best illustrated by FEM mode shape animation with color contours signifying the degree and polarity of rocking motion in each element. A snap shot of a rather exaggerated modal deflection is given in Figure 2-2. The basic concept of this degenerate rocking mode design is to counterbalance the post rocking momentum with opposing outer sensing plate momentum so that the underlying baseplate and mounting frame (with green contours) exhibit zero rocking or rotation. Outer resonator plate and inner post resonator are elastically tied to the baseplate via beam flexures with symmetry and some degree of commonality

such that two orthogonal, degenerate, differential rocking modes obtain.

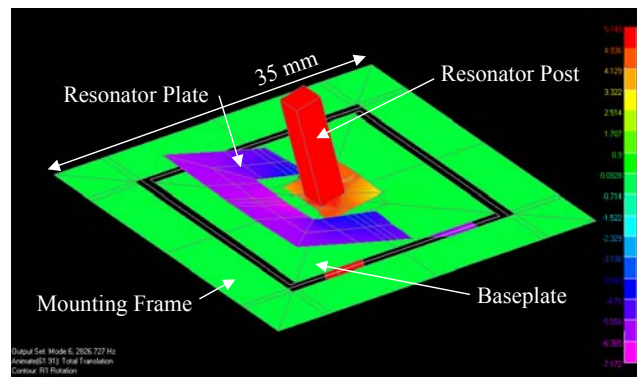


Figure 2-2: Mesogyro differential rocking mode

When one of the differential modes is driven say about the X axis an input rate along Z will couple momentum into the Y axis or output mode. The angular gain,  $k$  or figure of merit for this coupling is 1 for a Foucault pendulum or pure post resonator. For this mesogyro the plate has  $k=0$  and the post has  $k=1$  so the net angular gain is the average or  $k=1/2$ . For reference, the HRG the angular gain is 0.3.

An interesting aspect of this design is the opportunity to attain 'perfect' isolation by simply trimming the post length. It is readily shown by lumped mass modeling or by FEM study that for a given plate size and inertia there is an optimum post length that nulls the baseplate and frame motion, as illustrated in Figure 2.3.

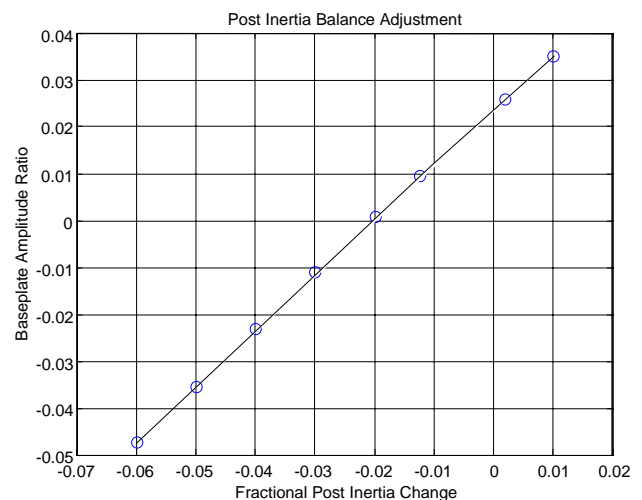


Figure 2-3: Base isolation vs. post inertia adjust from FEA.

In the course of the performance improvement phase above successive beam designs were devised to reduce loading and hence anchor losses of the bonds attaching the resonator to the baseplate. The final beam designs and electrode arrangement under the resonator are illustrated in Figure 2-4.

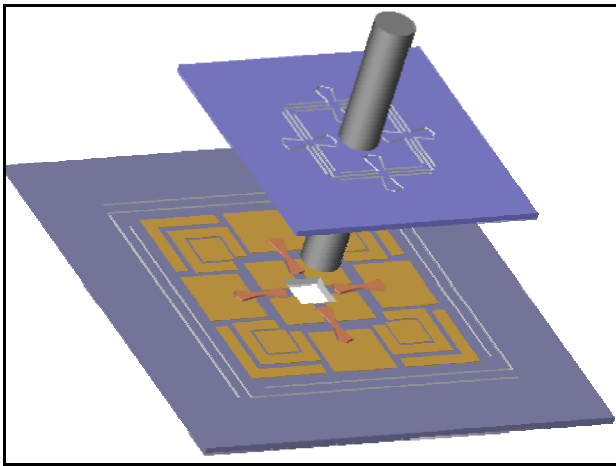


Figure 2-4 Mesogyro resonator, electrode baseplate and mounting frame design.

### 3. ELECTRICAL DESIGN

#### Overview of Operation

The mesogyroscope's analog electronics consists of three control loops (a drive loop, closed loop output, and a quadrature nulling loop), rate and quadrature demodulation circuits, and electrostatic tuning biases. This analog electronics interfaces with the physical mesogyroscope resonator via a 20-electrode pattern on the baseplate that makes a set of 20 capacitors with the doped, conductive resonator across the  $15\mu\text{m}$  gap between the baseplate wafer and bonded resonator wafer. The resonator itself is biased at a DC voltage of 14 volts.

A set of eight DC bias electrodes are used to tune the resonator (via electrostatic spring softening) such that its two differential-rock modes become degenerate in frequency. A set of drive pads are used to excite differential-rock vibration in the  $\theta_1$  direction (as shown in the Figure 3-1) with peak motion at the tip of the outer resonator plate being approximately  $2\mu\text{m}$ . This vibratory motion is kept constant via a positive feedback drive loop which automatically locks onto the natural frequency of the resonator. An analog Automatic Gain Control (AGC) circuit adjusts the gain in this drive loop to maintain a constant  $2\mu\text{m}$  rock amplitude.

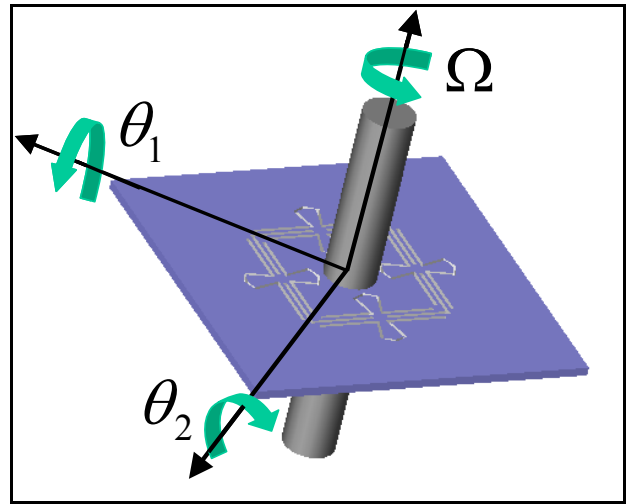


Figure 3-1 Mesogyro electronic control axes

Any inertial rotation of the gyroscope around the  $\Omega$  axis transfers vibratory energy into the  $\theta_2$  direction. Motion in the  $\theta_2$  direction is sensed via a set of pads feeding into transimpedance amplifiers. This motion in the sense ( $\theta_2$ ) direction is feed directly back with negative feedback, effectively nulling the transferred vibrational energy. The torque needed to null this motion encodes the inertial rate as an amplitude modulated signal in phase with the drive rock's motion ( $\theta_1$ ). Multiplying together and low-pass filtering the analog signals encoding the drive rock's motion and sense rock's rebalance torque generates a baseband analog voltage proportional to the inertial rate the gyroscope is undergoing about its input axis.

#### Baseplate Electrodes

Figure 3-2 shows the layout of the 20 electrodes patterned onto the mesogyro's baseplate along with descriptive labels.

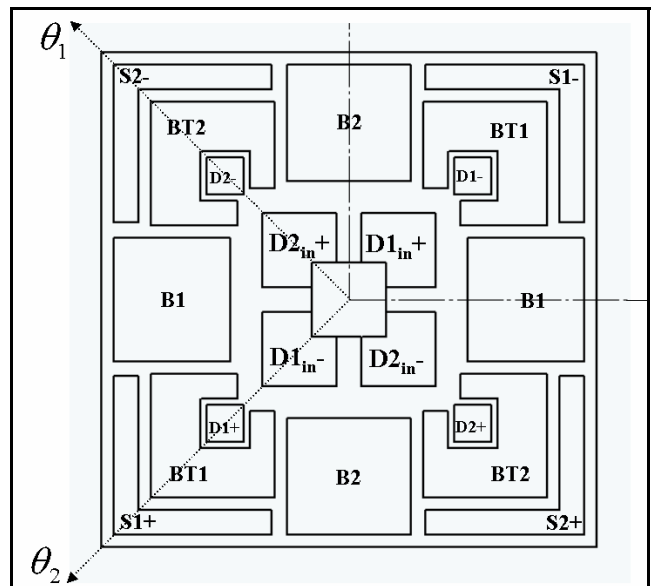


Figure 3-2 Baseplate electrode layout and nomenclature.

The four inner electrodes are positioned directly underneath the inner resonator plate, while the other 16 are beneath the resonator's outer plate (see exploded view in Figure 2-4 above). There are 8 drive electrodes (labeled 'D') in Figure 3-2. A sinusoidal voltage applied between any one of these electrodes and the resonator creates a torque in the resonator and thus excites the resonator's vibrational modes. Referring to the figure, the diagonal set of electrodes (D1+, D1<sub>in</sub>-, D1<sub>in</sub>+, D1-) are positioned to generate torques in the  $\theta_1$  direction. The areas of the electrodes and their moment arms with respect to the resonator have been designed such that if sinusoidal signals are input in the +/- labeled phases, then the differential-rock mode will be excited without exciting the common-rock (post and outer plate in phase) or other undesired vibrational modes of the gyroscope. This ability to prevent the analog electronics from "seeing" other resonance modes of this multi-degree-of-freedom structure allows for greatly simplified drive and sense loop designs (i.e. no extra filtering needed).

The diagonal set of electrodes (S1+, S1-) are paired to differentially sense motion along the  $\theta_1$  direction. These sense pads are fed into the virtual ground of transimpedance amplifiers (made with high input impedance op-amps). As the outer plate rocks, the capacitance between these sense electrodes and the resonator changes, forcing current into the transimpedance amplifiers. The resulting voltages are subtracted in an instrumentation amplifier generating a voltage signal proportional to the rocking motion in the  $\theta_1$  direction. Lead circuits are included between the transimpedance amplifiers and the instrumentation amplifier in order to correct for phase shifts in the transimpedance amplifiers.

The diagonal set of electrodes (BT1, BT1) are used to electrostatically soften restoring spring force in the  $\theta_1$  direction with only minimal softening off this direction. These two electrodes act equally on the resonator and thus get the same voltage and are labeled the same.

All of these diagonal drive, sense, and bias electrodes are mirrored in the  $\theta_2$  direction. Additionally, four electrostatic spring softening bias electrodes (B1, B1, B2, B2) are included in the horizontal and vertical directions. These electrodes are required to give full control over the resonator's spring matrix and thus achieve full modal degeneracy.

### Core Electronics

Figure 3-3 shows the core electronics of the mesogyroscope. The front-end sensing electronics shown was described in the previous section. It consists of four transimpedance amplifiers and two instrumentation amplifiers. The drive electrode phase and amplitude relationships are generated by four inverter circuits and voltage dividers. Two analog multiplier IC's are included in the core electronics to form the sense/force rebalance and

drive loops. Input voltages  $M_1$  and  $M_2$  control the gain and phase (positive feedback vs. negative feedback) of these loops.

Notice that the core electronics are perfectly symmetric with respect to the  $\theta_1$  and  $\theta_2$  directions, meaning that the drive and sense axes can be reversed electronically. This feature of the electronics was included to allow easy tuning of the device and to allow compensation of damping induced rate drift which is cancelable to first order using this drive axis switching technique. In the complete electronics, a set of analog switches were included to allow fully electronic gain and loop switching so that the drive and sense axes could be reversed via a single digital control line's level shift.

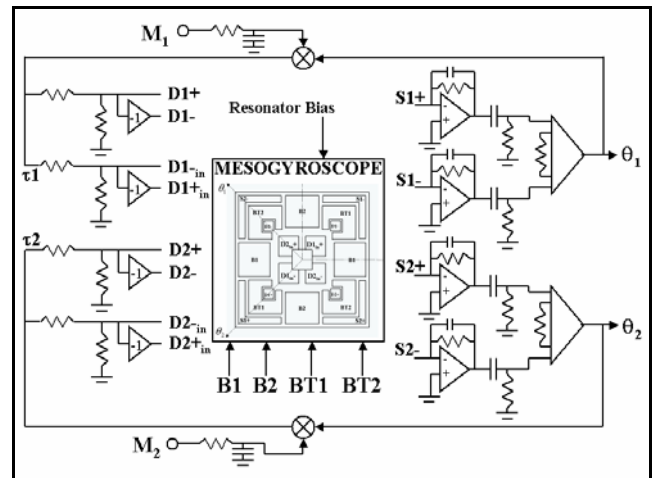


Figure 3-3 Mesogyro core electronics

### Full Mesogyroscope Electronics

Figure 3-4 below shows the rest of the analog electronics for the mesogyroscope. The AGC block controls the drive loop gain via  $M_1$ . The output closed loop (force to rebalance) gain is set simply by putting a constant DC voltage into  $M_2$ . The gyroscope's final rate output signal is generated by the synchronous demodulation of the  $\theta_1$  and  $\theta_2$  signals via the circuit shown. An additional demodulation of the sense ( $\theta_2$ ) signal with a  $90^\circ$  phase shifted copy of  $\theta_1$  produces the quadrature signal (a measure of improper stiffness coupling between the modes). Feeding this quadrature signal back via a PI controller to the B2 tuning bias automatically nulls this stiffness coupling. Finally, the  $\theta_1$  signal itself is output to any testing or IMU electronics for temperature compensation algorithms to use.

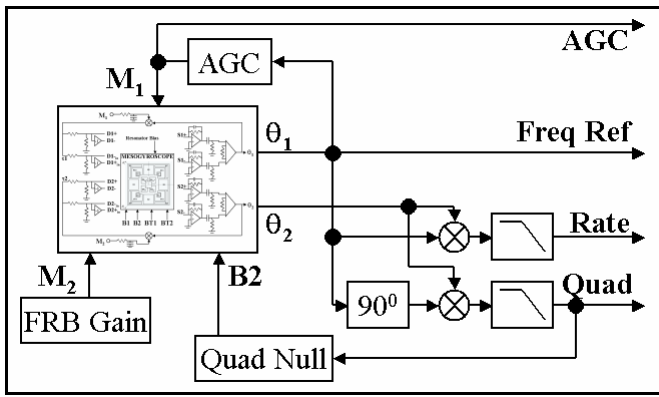


Figure 3-4 Mesogyro analog control electronics

#### 4. SILICON FABRICATION

The meso-gyro is designed to be a precision fabricated device, with large inherent sensitivity, isolated from external noise sources. By building the device at meso scale one obtains the benefit of using micro-machining fabrication techniques on a meso-scale device, allowing batch fabrication of die while attaining large relative precision; another benefit attained is the ability to design in large area capacitive sense and drive pads, allowing for precision, electronic sense and tuning of the device. The counter rocking feature of the gyro makes the system a net zero angular momentum system, thus minimizing coupling effects through the package. Built in silicon isolation springs assure that what coupling does occur will only take place at very low frequencies.

The sensor part of the meso-gyro is fabricated using standard bulk micro-machining processes. Two silicon

plasma etched to define the geometry of the gyro. They are then metalized to form the drive and sense pads, the electrical lines and the bond pads. The resonator and base plate are then Si-Au eutectically bonded together. Pyrex posts are then anodically bonded to the top and bottom of the resonator. The Pyrex posts are the part of the gyro which couples to the Coriolis force. The fabrication process is illustrated in the figure below.

The gyro is a two degree of freedom, resonant, vibratory system. The coupling between the two modes is maximized when the resonant frequencies of the two modes are identical. If the frequencies are matched, the gyro is said to be degenerate. Symmetry of design by itself is insufficient to attain degeneracy; symmetry of construction is necessary as well. In particular, the bonds between the resonator and baseplate must be of near identical quality and construction.

Several design iterations have resulted in a robust fabrication process with a greater than 50% yield of die that are degenerate to within 0.2%. Typical “Q” factors were measured to be approximately 10,000.

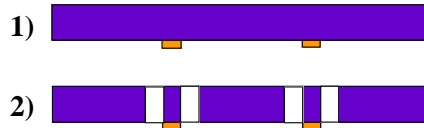
Device yield and quality degraded appreciably with the anodic bonding of the post. Yields from the post bonding process were approximately 25% for devices degenerate to within 1%. Typically, “Q” values would increase with the bonding of the post to approximately 15,000.

Improving the yield and quality of the post bonding process is an ongoing issue. It is also a bottleneck in the fabrication process in the sense that it is not amenable to batch fabrication technique. Ultimately, one would like to vacuum package the gyros via some batch assembly process. Before this can be accomplished, issues with the post bonding process will need to be resolved.

#### Sensor fabrication process

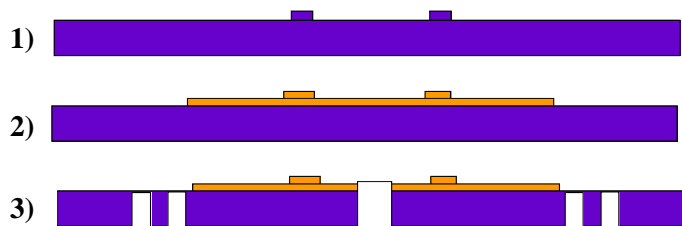
##### Resonator fabrication process:

- 1) Metalize to form bond pads
- 2) STS (deep RIE) etch to define springs



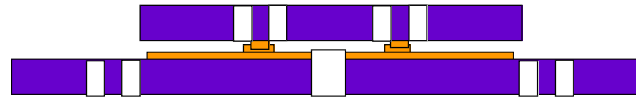
##### Baseplate fabrication process:

- 1) Pillars defining bond sites etched
- 2) Drive/sense pads, electrical lines and bond pads defined by metalization
- 3) STS (deep RIE) etch to define clearances and isolation springs



wafers (the resonator and the baseplate) are wet etched and

**Resonator is eutectically bonded to baseplate**



**Pyrex posts are anodically bonded to resonator**

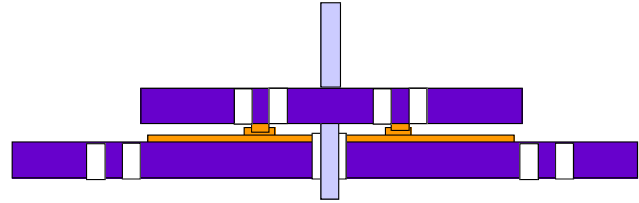


Figure 4-1b Fabrication Process (wafer bonding)

### 5. ASSEMBLY & PACKAGING

After the post attachment process the gyro is bonded to an aluminum nitride substrate and wire bonded. This is then bonded into a Kovar housing and wire bonded to I/O pins. The lid for the package is welded, the assembly is pumped down to a pressure of  $10^{-8}$  torr, and the pinch-off tube is sealed. An exploded view of the assembly is shown below.

All materials were chosen for thermal and vacuum compatibility. Thermal mechanical testing was performed on the adhesive used at the gyro/substrate interface, and also at the substrate/housing interface to ensure that it would not be a source of hysteresis during temperature cycling. A

thermally activated getter was designed in to reduce, if needed, the pressure within the package due to any residual outgassing.

All of the electronics for the gyro assembly currently reside on two PWBs outside of the vacuum package. This prototype version of the vacuum package was deliberately designed oversized to allow for maximal flexibility when incorporating the electronics into the package in the future. A custom ASIC is being designed for the gyro. Following optimization of the electronics and the ASIC, package volume can be reduced.

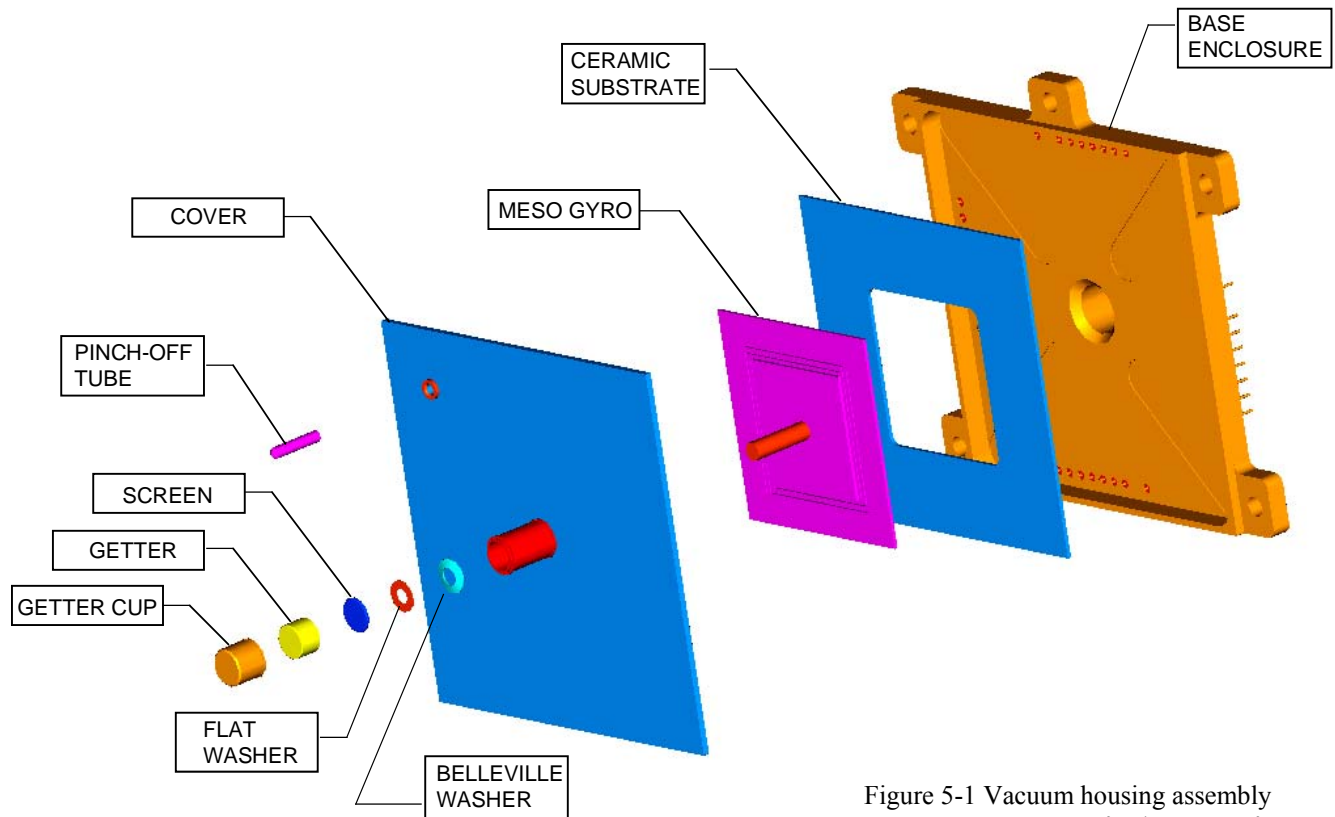


Figure 5-1 Vacuum housing assembly  
Boeing/JPL Proprietary

## 6. TEST METHODS & RESULTS

Figure 6-1 illustrates the current Mesogyro test flow. The first three tests are nearly identical; as such they will be discussed together in the first subsection. The Packaged Gyro Testing will then be discussed.

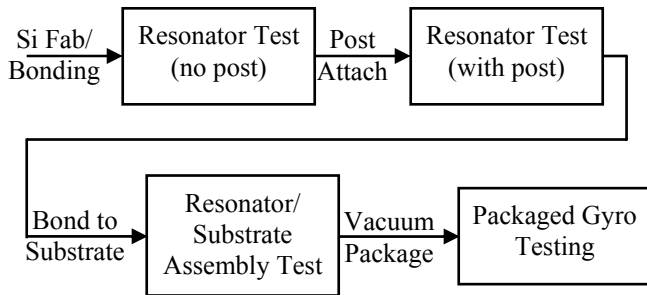


Figure 6-1: Mesogyro Test Flow

*Resonator Tests – (no post, with post, Resonator/Substrate Assembly)*

The purpose of the resonator tests is to screen devices after each step in the manufacturing/assembly flow, according to two criteria:

- (1) frequency split between natural rocking modes of less than 10 Hz
- (2) Q of rocking modes of at least 10,000

Resonators that satisfy these two criteria can be electrostatically tuned to function as high-performance gyroscopes. The chief difference between the three instances of this test is the fixturing required to provide the  $V_{bias}$  and Drive signals to the device. Figure 6-2 shows the test equipment setup for these tests.

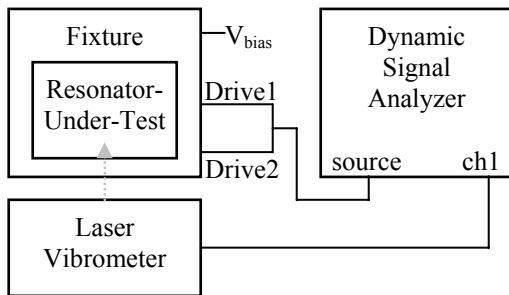


Figure 6-2: Equipment Setup for Resonator Tests

The DSA is set to source a random noise signal, which drives the resonator. The laser vibrometer converts the resulting motion of the resonator to a signal that the DSA can use to generate a frequency response, from which the natural rocking modes can be identified and measured.

### Packaged Gyro Testing

Packaged gyros are integrated with drive and sense electronics for this testing. The signal interface is shown in Figure 6-3.

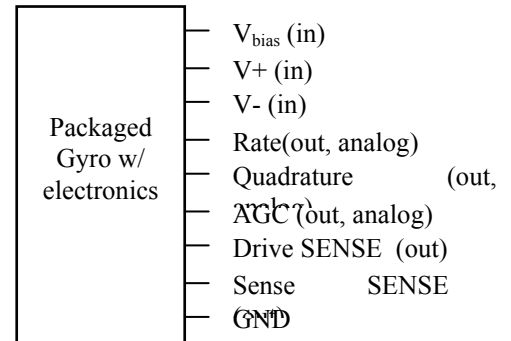


Figure 6-3: Interface to packaged gyro/electronics

Noise performance is quantified using the Green Chart. Figure 6-4 is the Green Chart (at ambient temperature) from the best performing gyro to date.

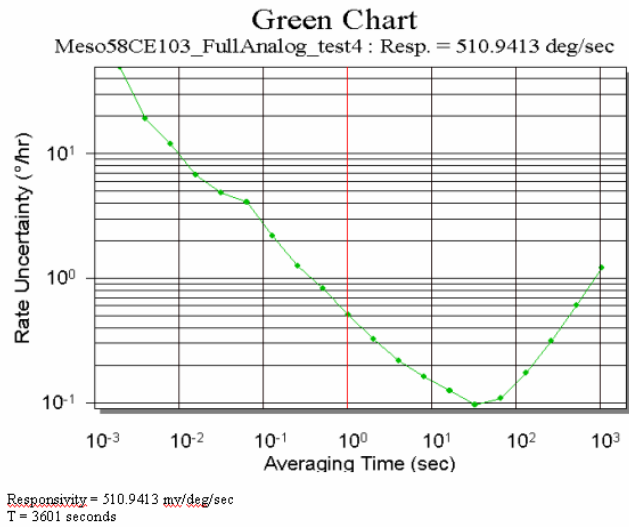


Figure 6-4: Green Chart – Ambient Temperature

The following performance figures can be extracted:

Bias Instability	0.1 [deg/hr]
ARW	0.008 [deg/√hr]

Testing has also been performed over temperature (-55 to +85°C). Figure 6-5 shows the linear relationship between the temperature and the rocking frequency of the device and Figure 6-6 shows the uncompensated zero rate bias of the best performing device to date, over temperature, using rocking frequency as the indicator of temperature. The ~140 deg/h of non-repeatability over temperature is attributable to internal losses and not packaging stresses.

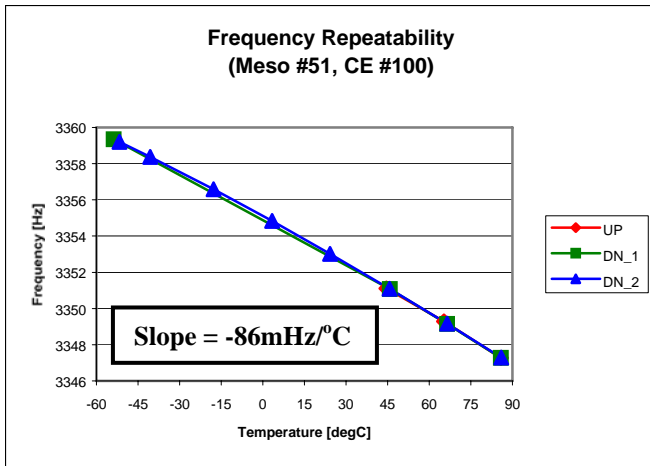


Figure 6-5: Rocking Frequency vs. Temperature

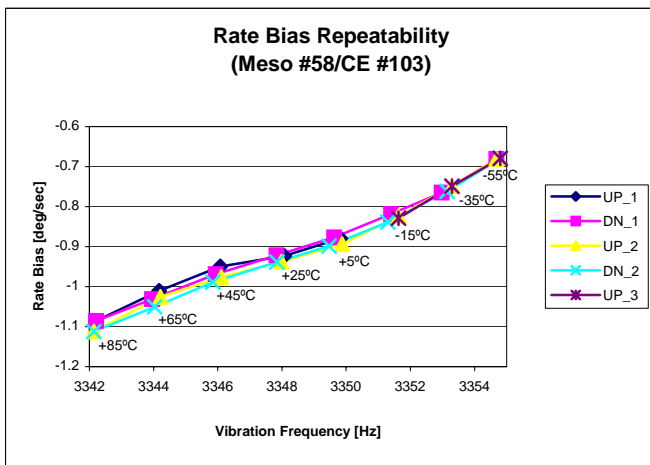


Figure 6-6: Zero Rate Bias Over Temperature (Uncompensated)

The final mesogyro assembly for testing is shown in Figure 6-7. The vacuum packaged mesogyro is mounted to an aluminum block with its core electronics PWB on the top pin side of the package. The control electronics is mounted on a side fixture for convenient access during testing. In final use this board is mounted on top of the core electronics yielding a unit of ~2.4 in x 2.4 in x 1 in.

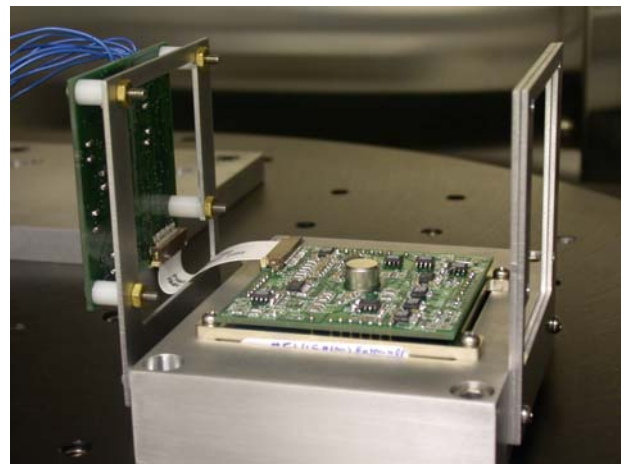


Figure 6-7 Assembled mesogyro in test configuration.

## 7. CONCLUSIONS

The first micromachined silicon gyroscope at mesoscale is described. A novel isolated post resonator gyro design is employed to provide a large measure of independence from the case. The much higher mesoscale precision as well as larger capacitive area enabled significantly improved angle random walk, 0.008 deg/rt-h and bias stability, 0.1 deg/h or 10X improvement over previous MEMS microgyros. Temperature testing validated the isolated design independence of package stresses. Residual internal losses are believed to be limiting performance and temperature repeatability while the post assembly process is limiting overall yield and throughput. Improvements in these particular areas are thus recommended.

## REFERENCES

- [1] N. Yazdi, F. Ayazi, and K. Najafi, "Micromachined inertial sensors," *Proc. IEEE*, vol. 86, no. 8, pp. 1640–1659, Aug. 1998.
- [2] A. Madni, L. Costlow, and R. Jaffe, "Aerospace technology and low automotive costs benefit quartz micromachined gyros," in *Proc. ION 57th Annu. Mtg. CIGTF 20th Biennial Guidance Test Symp.*, Albuquerque, NM, June 2001.
- [3] Kubena, R. et al, "Tunneling Rate Sensor", US Patent 5,756,895
- [4] T. K. Tang, R. C. Gutierrez, J. Wilcox, C. Stell, V. Vorperian, R. Calvet, W. Li, I. Charkaborty, R. Bartman, W. Kaiser, "Silicon Bulk Micromachined Vibratory Gyroscope", Tech Digest, Solid-State Sensor and Actuator Workshop, Hilton Head, S. C. pp. 288-293, June 1996.

